A terminating-type MEMS microwave power sensor and its amplification system

2010 J. Micromech. Microeng. 20 075021

(http://iopscience.iop.org/0960-1317/20/7/075021)

J. Micromech. Microeng. **20** (2010) 075021 (8pp) doi:10.1088/0960-1317/20/7/075021

A terminating-type MEMS microwave power sensor and its amplification system

De-bo Wang and Xiao-ping Liao[1]

Key Laboratory of MEMS of Ministry of Education, Southeast University, Nanjing 210096, People's Republic of China

E-mail: xpliao@seu.edu.cn

Received 5 March 2010, in final form 11 May 2010
Published 9 June 2010
Online at stacks.iop.org/JMM/20/075021

Abstract

A terminating-type MEMS microwave power sensor and its amplification system are presented in this paper. A SPICE model is introduced to simulate temperature distribution of this power sensor, and the model has a reference value to estimate the sensitivity of the power sensor. This power sensor is designed and fabricated using MEMS technology and the GaAs MMIC process. It is measured in the frequency range up to 20 GHz with an input power in the 0 to 50 mW range. Over the 50 mW dynamic range, the sensitivity is about 0.29, 0.24 and 0.22 mV mW^{-1} at 5, 10 and 15 GHz, respectively. The output voltage of the power sensor ranges from 0.64 to 15.2 mV at 5 GHz. After amplification, the output voltage ranges from 0.19 to 6.56 V. The amplification gain is about 437.5, and the sensitivity is increased to 1274 mV mW^{-1}. At 15 GHz, the output voltage of the power sensor ranges from 0.57 to 11.69 mV. After amplification, the output voltage ranges from 0.146 to 5.02 V. The amplification gain is about 438, and the sensitivity is increased to 974.8 mV mW^{-1}. The measurement results show that the amplification system can amplify the output weak signal of the power sensor well and have good linearity.

(Some figures in this article are in colour only in the electronic version)

1. Introduction

Microwave power measurement is an important part of microwave wireless applications such as modern personal communication systems and radar systems. Thermocouple-based power sensors have been one of the most widely used devices for microwave power measurement [1, 2]. The fabrication of these thermoelectric power sensors generally has two technologies: CMOS integrated circuit (IC) technology combined with an oriented etching technique and GaAs bulk micromachining technology. The standard CMOS technology cannot be used for microwave applications because of the lossy nature of a silicon substrate at microwave frequencies. Currents induced in the substrate result in unwanted frequency-dependent losses and dispersive characteristics due to electromagnetic coupling. At the same time, the standard CMOS IC technology is not suitable for the design of thermoelectric devices such as thermocouples. In order to reduce these inefficiencies, in the work of Milanovic *et al* [3], the silicon substrate has been removed from directly beneath the thermal and microwave structures. In the work of Jaeggi *et al* [4], the thermoelectric ac power sensor has been realized by industrial CMOS IC technology combined with one subsequent maskless etching step. The burn-out power of the sensor is 50 mW.

GaAs is chosen as the basic electronic and micromechanical semiconductor material because of its lower thermal conductivity, higher saturation velocity of electrons and higher temperature working conditions compared with silicon. Another significant advantage is that it can be integrated with MMICs and other planar connecting circuit structures. In the work of Dehe *et al* [5], GaAs bulk micromachining combined with MESFET technology has been applied to fabricate a thermoelectric microwave power sensor in a terminating load configuration. In the work of Lalinsky *et al* [6], a 2 μm thick GaAs cantilever beam of the power sensor microsystem has been investigated. Due to a very thin cantilever, high power–temperature conversion efficiency is achieved.

[1] Author to whom any correspondence should be addressed.

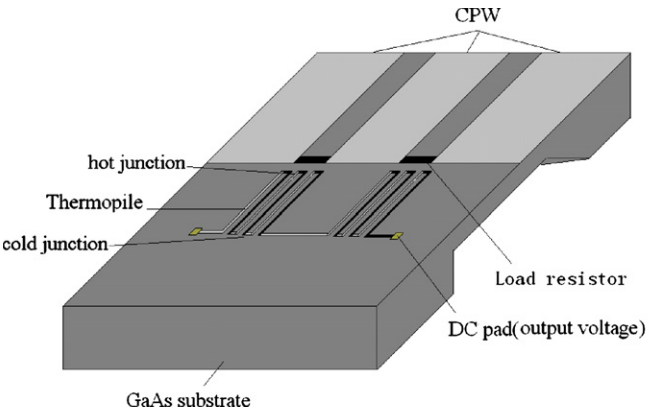

Figure 1. The structure of the power sensor.

In the above-mentioned thermoelectric power sensors, the main design emphasis is to obtain as high sensitivity as possible through a complex process. But the improvement is limited and increases the difficulty of the process. Another approach to improve the sensitivity is to design the amplification system of the power sensor. There is scarcely any published literature to propose the amplification system of the power sensor. In this work, an amplification system is proposed to amplify the output weak signal of the microwave power sensor based on hybrid integrated circuits. The novelties of this work are as follows: firstly, the power sensor is fully compatible and fabricated with a GaAs MMIC foundry process and the cost of the entire system is low. Secondly, only for the power sensors, the power–temperature–voltage conversion efficiency and the sensitivity can be improved through the complex process [5, 6]. Some researches about power–temperature–voltage conversion efficiency have been reported in our previous work [7]. But the complexity and the cost of process are increased, and the output voltage of the power sensors is still at an mV level. It cannot drive the load, overcome noise and provide a logic level for digital circuits. The output voltage after amplification can achieve a V level, and it can drive the load, overcome noise and provide a logic level for digital circuits. In section 2, the temperature distribution of this power sensor is given. In section 3, this power sensor is designed and fabricated. The measurement results of this power sensor are shown in section 4.

2. Principle and model

A major advantage of the thermoelectric conversion is its exact physical definition and inherent broad frequency range. The power sensor consists of a coplanar waveguide (CPW), load resistor, thermopile and dc pad as shown in figure 1. A CPW feeds the microwave signal to the power sensor. The load resistor absorbs the microwave power and converts it into heat. The resulting temperature is detected by the thermopile, which generates a dc voltage based on the Seebeck effect. The dc voltage is output by the dc pads. The output voltage is proportional to the microwave power. The output voltage and the sensitivity of the microwave power sensor are represented, respectively, as

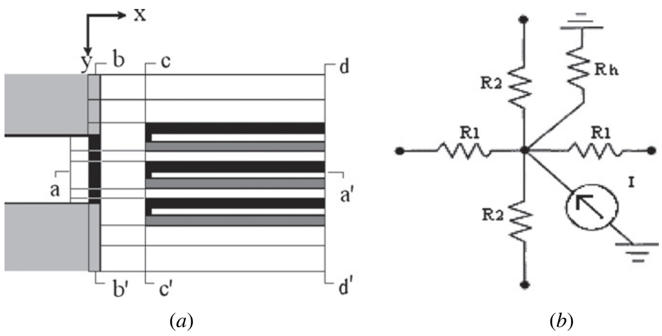

Figure 2. (*a*) Schematic view and (*b*) circuit element of the power sensor.

$$V_{\text{out}} = \alpha \sum_{i}^{N} (T_h - T_c) \tag{1}$$

$$S_{\text{th}} = V_{\text{out}}/P_{\text{diss}}, \tag{2}$$

where α is the Seebeck coefficient, P_{diss} is the microwave power dissipated by the load resistor, N is the number of the thermopile, T_h and T_c are the temperatures of the hot and cold junctions of the thermopile, respectively.

In the work of Swart and Milanovic [8, 9], the SPICE equivalent circuit has been used to simulate the heat-transfer behavior and the temperature distribution of the power sensor. The thermal flow is represented as a current and the temperature as a voltage. In our work, the thickness of the membrane is much smaller than the dimensions of this power sensor. Therefore, the steady-state heat transfer is considered in the x–y coordinate system. Due to the symmetrical structure, only half of this power sensor is considered. The 2D layout is further subdivided into smaller elements, as shown in figure 2(*a*). Each circuit element is shown in figure 2(*b*), in accordance with the work of Swart and Milanovic, which includes convection, conduction and heat generation. The current source is only applicable for the load resistor which dissipates power and generates heat. The conductive transfer by a thermal resistor is represented as

$$R_{1,2} = l/\lambda A, \tag{3}$$

where l is the length, λ is the thermal conductivity and A is the cross section.

The convective resistor is represented as

$$R_h = 1/hA_s, \tag{4}$$

where h is the surface coefficient of heat transfer and A_s is the surface area. The symbol for ground in figure 2(*b*) represents the ambient temperature, 300 K in this paper.

The cross-section view of the power sensor is shown in figure 3. The symbols d_1, d_2 and d_3 are the thicknesses of the load resistor, the thermopile and the GaAs substrate, respectively. l_1 is the length of the load resistor. l_2 is the distance between the hot junction and the load resistor. l_3 is the length of the thermocouple. Because the 3D structure

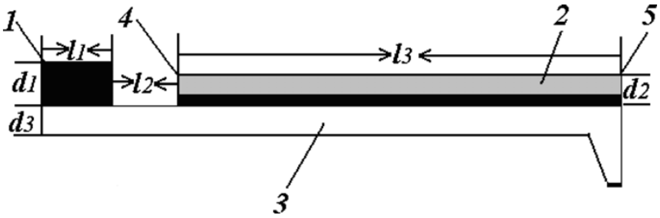

Figure 3. Cross-sectional view of the power sensor: (1) load resistor; (2) thermopile; (3) GaAs substrate; (4) hot junction and (5) cold junction.

Table 1. The values of the equivalent electrical elements.

	Substrate	CPW, substrate	Resistor, substrate	Thermopile, substrate
$R_1(\Omega)$	988.14	645.2	1010.77	1058.95
$R_2(\Omega)$	60.07	588.3	252.69	965.6
$R_h(\Omega)$	6.08×10^8	4.05×10^7	4.19×10^8	4.05×10^7

is treated as 2D in the layout plan, the thermopile and the substrate should be regarded as one material. The same holds true for the load resistor and the substrate. In this work, some equivalent quantities are introduced [10]. λ_{e1} is the equivalent thermal conductivity of the load resistor and the substrate, while λ_{e2} denotes the equivalent thermal conductivity of the thermopile and the substrate. They can be defined as

$$\lambda_{e1} = \frac{\lambda_1 d_1 + \lambda_3 d_3}{d_1 + d_3} \tag{5}$$

$$\lambda_{e2} = \frac{\lambda_3 d_3 + \lambda_2 \cdot \frac{d_2}{2}}{d_e} = \frac{\lambda_3 d_3 + \lambda_2 \cdot \frac{d_2}{2}}{d_3 + \frac{d_2}{2}}, \tag{6}$$

where d_e is the equivalent thickness of the thermopile and the substrate and $\lambda_2 = \frac{\lambda_p + \lambda_n}{2}$ is the average thermal conductivity of the thermocouple with λ_p and λ_n denoting the thermal conductivity of the positive and negative conductors of the thermocouple, respectively. According to the structure parameters of this power sensor, the equivalent electrical elements can be calculated as shown in table 1.

The equivalent circuit model is simulated using the SPICE with the constant current set to 100 mA, equal to an input power 20 dBm at 10 GHz. In the x direction as shown in figure 2(a), the larger the distance from the load resistor, the lower the temperature. The temperature distribution along a–a′ is an approximate linear decline as shown in figure 4, which is close to the expectation. The temperature distributions of the power sensor in the y direction along the load resistor b–b′, the hot junction c–c′ and the cold junction d–d′ are shown in figure 5. The highest values of the temperature are in the middle of the load resistor, and the peak value is nearly 325 K. The temperature distributions along the hot junction c–c′ and the cold junction d–d′ are similar to that of b–b′, but the peak values are 318 K and 302 K, respectively. From the simulation results of the temperature distribution, the sensitivity can be calculated by using equations (1) and (2). The sensitivity is approximately

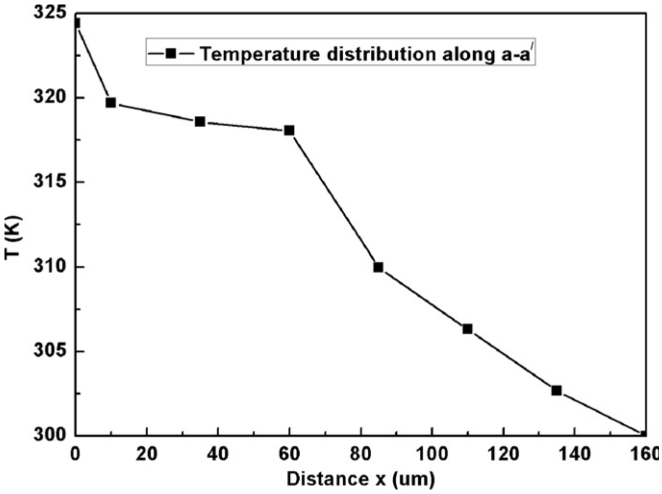

Figure 4. Temperature distribution in the x direction.

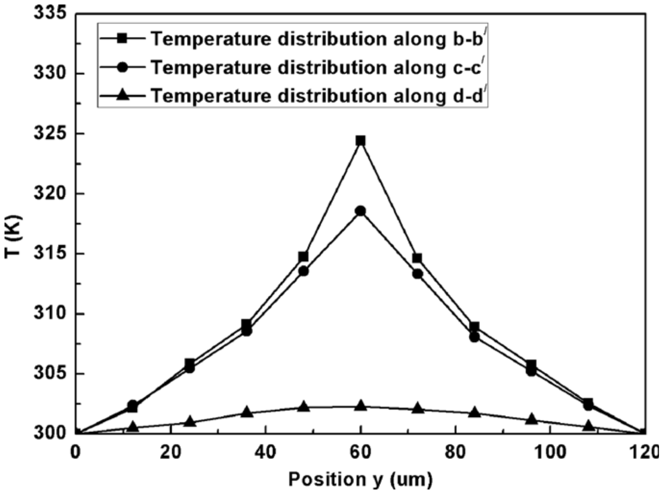

Figure 5. Temperature distribution in the y direction.

0.25 mV mW^{-1}. Therefore, the SPICE model has a reference value to estimate the sensitivity of the power sensor.

In order to study the temperature distribution further, it is also simulated with ANSYS as shown in figure 6. The input power is the same as that of SPICE, and the peak value of the temperature is 338 K. The temperature is a little higher than that simulated with SPICE, but the relative difference between them is below 4%, and the temperature distribution is the same.

3. Design and fabrication

The fabrication of this power sensor is compatible with the GaAs MMIC process [11]. In this power sensor, the CPW is designed to have 50 Ω characteristic impedance. The width of the center conductor is designed to be100 μm, and the slot is designed to be 58 μm between the center conductor and the ground line. The thermocouples are formed utilizing the n+ GaAs layer for one leg and an Au interconnect for the

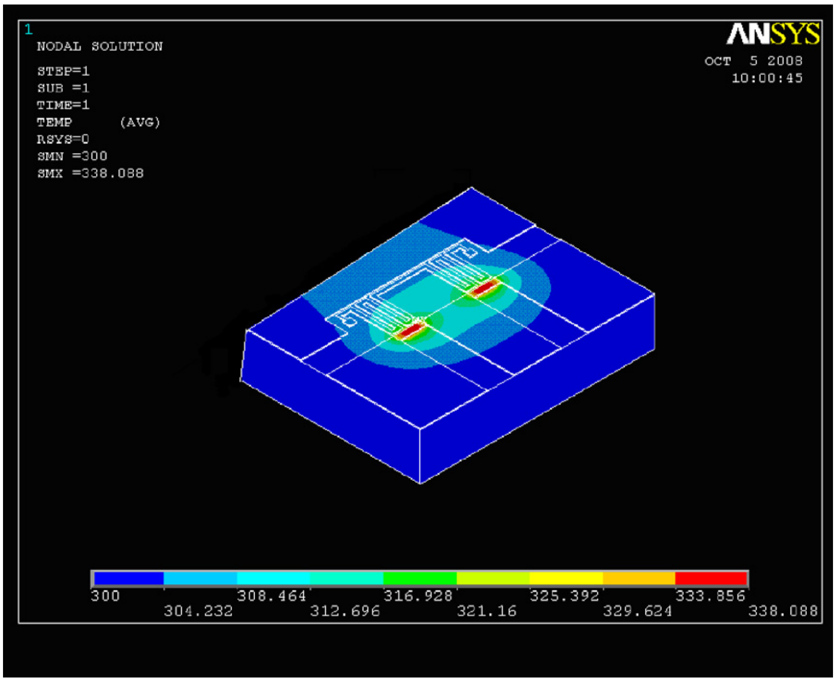

Figure 6. Temperature distribution with ANSYS.

second leg at the hot junction, and a temperature difference is maintained between the hot junction and the cold junction, and then a dc voltage is developed between the dc pads at the cold junction. The thermocouples connected in series constitute a thermopile. The longer the length of the thermopile, the higher the sensitivity, but the response time and the thermal resistance increase. The greater the number of thermocouples in the thermopile, the higher the sensitivity, but the thermal radiation loss and the thermal noise increase. According to equation (2), the sensitivity of the microwave power sensor is represented as

$$S = \frac{V_{\text{out}}}{P_{\text{diss}}} = (\alpha_1 - \alpha_2)\frac{\eta N S}{\lambda_{e2} p}\tanh(pL), \qquad (7)$$

where α_1 and α_2 are the Seebeck coefficients of GaAs and Au, respectively, η is the efficiency of energy absorption for the CPW, S is the area of the thermopile and $P = \frac{h}{\lambda_{e2} d_2}$, and it determines the decline rate from the peak speed of thermopile temperature. According to equation (7), the length and number of the thermopile are optimized as shown in figure 7. The optimal values of the thermopile length and number are 150 μm and 12 pairs, respectively. A trade-off has to be made between the microwave performance and the thermal performance of the sensor for the distance of the thermopile away from the load resistor. The distance is designed to be 10 μm.

The process steps of the power sensor are briefly described as follows.

(1) The thickness of the GaAs supporting layer is 500 μm. AlGaAs thin film and n+ GaAs are epitaxially grown. The AlGaAs thin film is used as the etch-stop layer. The n+ GaAs is made of a 2500 Å thick epitaxial layer for one leg of the thermopiles with a Seebeck coefficient of 200 μV K^{-1}.

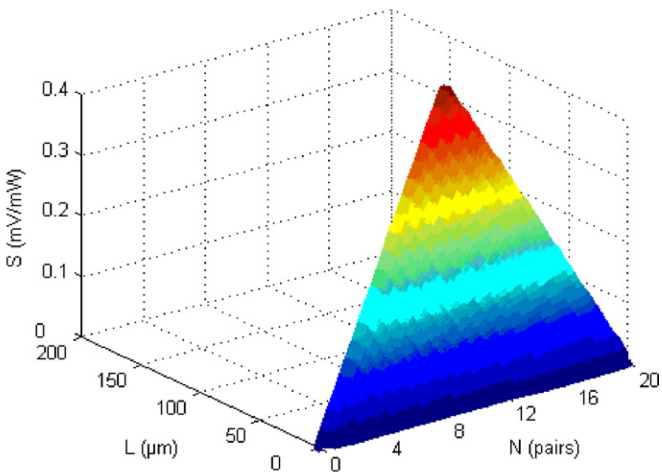

Figure 7. Optimal parameters for the thermopile.

(2) The AuGeNi/Au layer is sputtered for the second leg of the thermopiles by using a lift-off process through evaporating the 500/2200 Å thickness. The role of the AuGeNi/Au layer is to form an Ohmic contact [12] with the n+ GaAs. An important issue in the design is to keep the Ohmic resistance of the thermopiles as low as possible since it determines the signal to noise ratio and the dynamic range of the sensor.

(3) The load resistor is made by using a lift-off process through depositing a TaN layer with a square resistance of 25 $\Omega/\square$. The width of the load resistor is 14.5 μm since the slot of the CPW is fixed at 58 μm.

(4) A 500/1500/300 Å Ti/Au/Ti seed layer is sputtered and patterned. The role of the Ti/Au/Ti seed layer is to

enhance the adhesion between the Au and the substrate and prevent the Au from giving off when bonding.

(5) After removing the top Ti layer, the transmission lines of the CPW are formed through electroplating a 2 μm thick Au layer.

(6) The substrate thickness is reduced to 100 μm.

(7) The substrate is etched back to the AlGaAs layer.

The process steps of the power sensor are shown in figure 8. The SEM image of the power sensor is shown in figure 9.

4. Measurements

The power sensor is measured at different input powers and different microwave frequencies. First, in order to obtain an estimate of the input mismatch error of the power sensor, the return loss is measured. Second, in order to obtain the frequency dependence characteristic of the power sensor, a frequency dependence measurement is taken. Third, in order to obtain the sensitivity of the power sensor, the sensitivity before amplification is measured. Fourth, in order to obtain the sensitivity of the power sensor after amplification, the sensitivity measurement after amplification is finished.

4.1. Return loss measurement

Return loss of this power sensor is measured using a network analyzer and a Cascade Microtech 1200 probe station. These are used to determine the input mismatch error over the entire frequency (0–20 GHz) range. The measurement results include parasitic effect of the pad and underlying substrate, and it is below −26 dB over the entire frequency range as shown in figure 10. This reflects that the power sensor has a good match characteristic.

4.2. Frequency dependence measurement

For a frequency dependence measurement, the microwave signals are applied to the power sensor with a frequency in the range of 1 to 20 GHz at 10 dBm, and the output voltage is recorded as shown in figure 11. Due to the electromagnetic coupling loss of the CPW at microwave frequencies [13], the power absorbed by the load resistor is not the ideal input power. As the frequency increases, the CPW suffers from dispersion loss caused by air–dielectric material discontinuity which is inherent to substrate-supported transmission lines. In addition, in the microwave frequency range [14], the load resistor is not a pure resistor due to the parasitic effect, which includes parasitic capacitance and parasitic inductance. The capacitance and the inductance will store some microwave power. The microwave power stored is not used by the load resistor, which is the reason why the parasitic loss of the load resistor exists. Furthermore, the parasitic loss of the load resistor increases with the microwave frequency. So the output voltages result in unwanted frequency-dependent losses. As the power loss increases with the microwave frequency, the microwave power absorbed by the load resistor decreases. So the output voltage decreases with the microwave frequency as shown in figure 11.

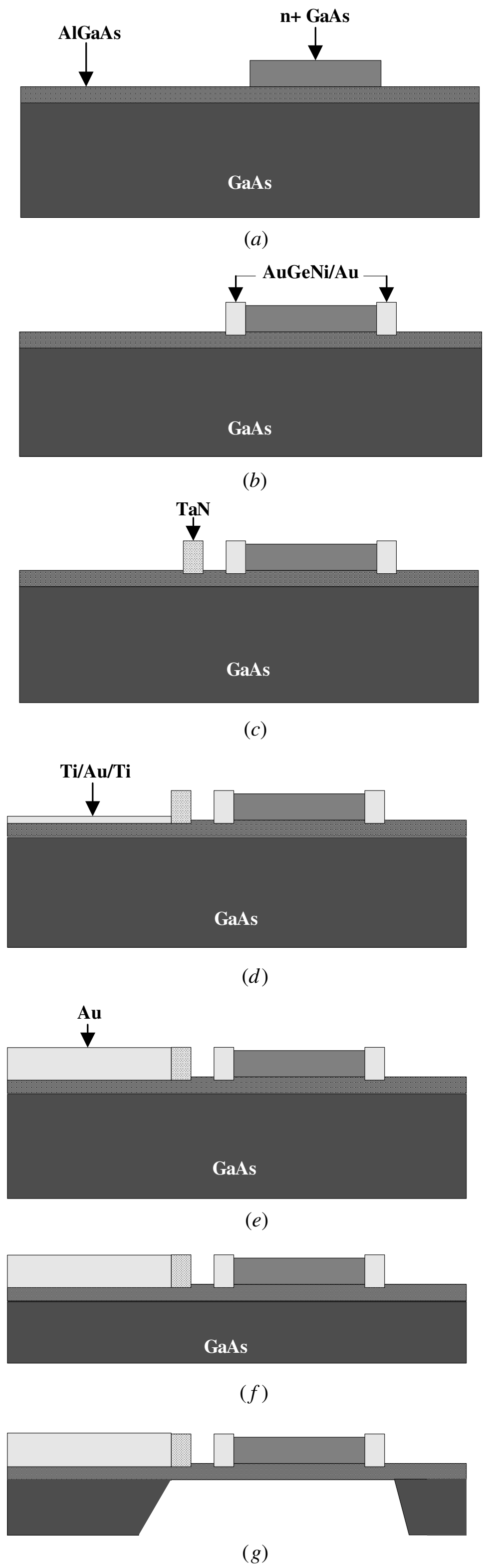

Figure 8. Process steps during fabrication: (*a*) epitaxial growth of AlGaAs thin film and n+ GaAs, (*b*) sputtering of AuGeNi/Au, (*c*) deposition of TaN, (*d*) sputtering of Ti/Au/Ti, (*e*) electroplating of Au, (*f*) subtraction of substrate, (*g*) etching back.

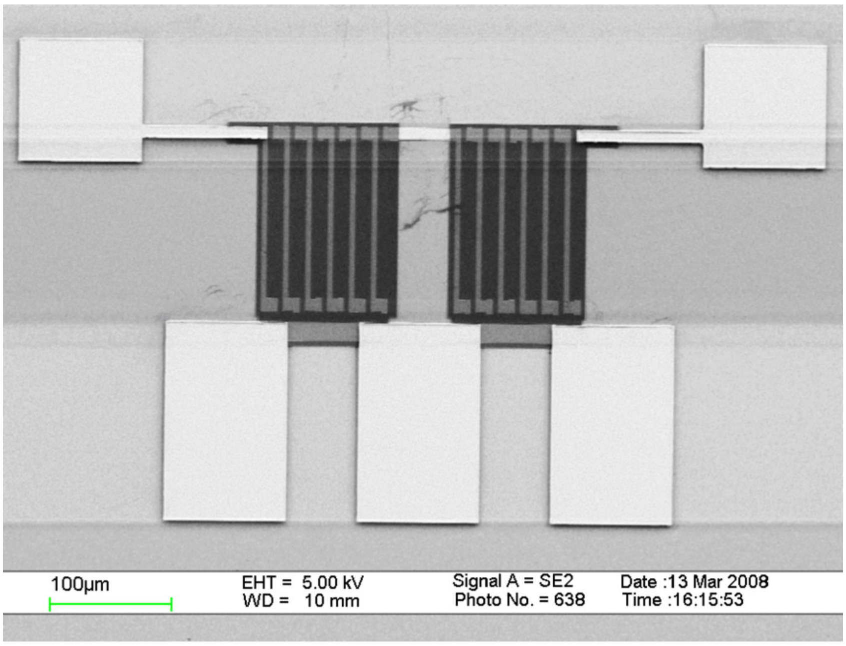

Figure 9. SEM image of the power sensor.

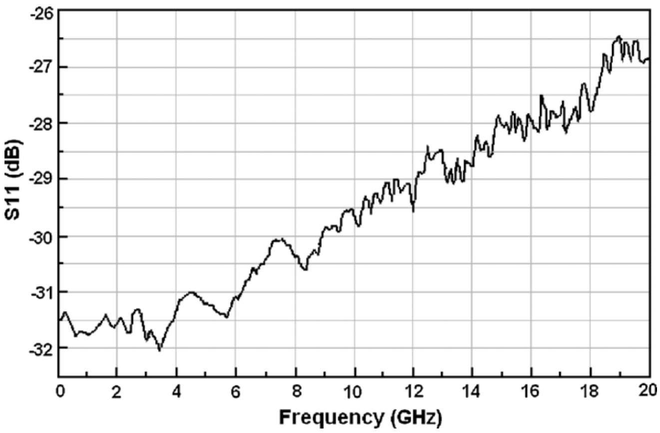

Figure 10. Measured return loss versus frequency characteristics.

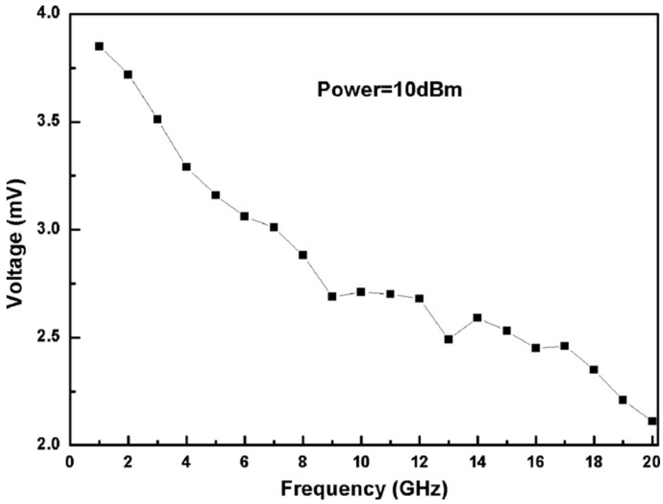

Figure 11. Measured frequency dependence of the output voltage.

4.3. Sensitivity measurement before amplification

For a sensitivity measurement of this power sensor before amplification, the microwave signals are applied to the power sensor with a power in the range of 0 to 17 dBm (50 mW) at 5, 10 and 15 GHz, and the output voltage is recorded. The measurement results are shown in figure 12. The output voltage increases with the input microwave power. The output voltage results in unwanted frequency-dependent losses due to the electromagnetic coupling loss of the CPW and the parasitic loss of the load resistor. Especially, when the input microwave power increases, the differences become larger. The sensitivity is about 0.29, 0.24 and 0.22 mV mW^{-1} at 5, 10 and 15 GHz, respectively. The results of the sensitivity are of the same order of magnitude between the measurement and the simulation, so the model in section 2 has a reference value to estimate the sensitivity. The measurement results show that the power sensor has good linearity.

4.4. Sensitivity measurement after amplification

As the output signal of the microwave power sensor is relatively weak, in order to facilitate the signal processing of the following circuit, the weak signal of the power sensor needs to be amplified. The amplification system consists of an amplifier circuit, a low-pass filter circuit and a printed circuit board as shown in figure 13. The gain of the amplifier circuit is designed to be 500, and the cut-off frequency of the low-pass filter circuit is 50 Hz. The measurement result of the

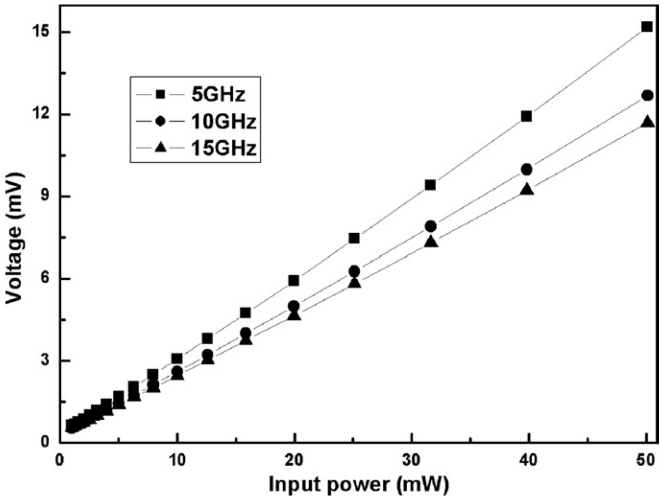

Figure 12. Measured output voltage versus input power characteristics before amplification.

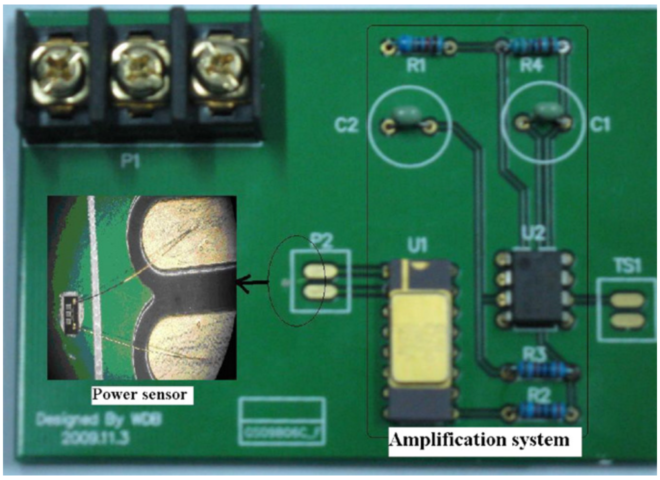

Figure 13. The printed circuit board of the system.

amplification system is shown in figure 14. The input voltage is 19.2 mV and the output voltage is 10.4 V. The gain of the amplification system is about 540.

The insets in figures 15(*a*)–(*c*) show the output voltage of the power sensor before amplification at the same frequency with the output voltage of the power sensor after amplification in figures 15(*a*)–(*c*). The measurement results at 10 GHz are shown in figure 15(*a*). The output voltage increases with the input power. When the input power is within 50 mW, the output voltage has good linearity. However, when the input power is more than 50 mW, the linearity of the output voltage becomes bad. The main reason is that the operational amplifier in the amplification system would reach saturation when the input power is more than 50 mW. Within 50 mW, the measurement results at 5 and 15 GHz are shown in figures 15(*b*), (*c*). The output voltage of the power sensor ranges from 0.64 to 15.2 mV at 5 GHz. After amplification, the output voltage of the amplification system ranges from 0.19 to 6.56 V. The gain is about 437.5, and the sensitivity is increased to 1274 mV mW^{-1}. At 15 GHz, the output voltage of the power sensor ranges from 0.57 to 11.69 mV. After amplification, the output voltage of the amplification system ranges from 0.146 to 5.02 V. The gain is about 438, and the sensitivity is increased to 974.8 mV mW^{-1}. The measurement results show that the amplification system can amplify the output weak

Figure 14. The measurement result of the amplification system.

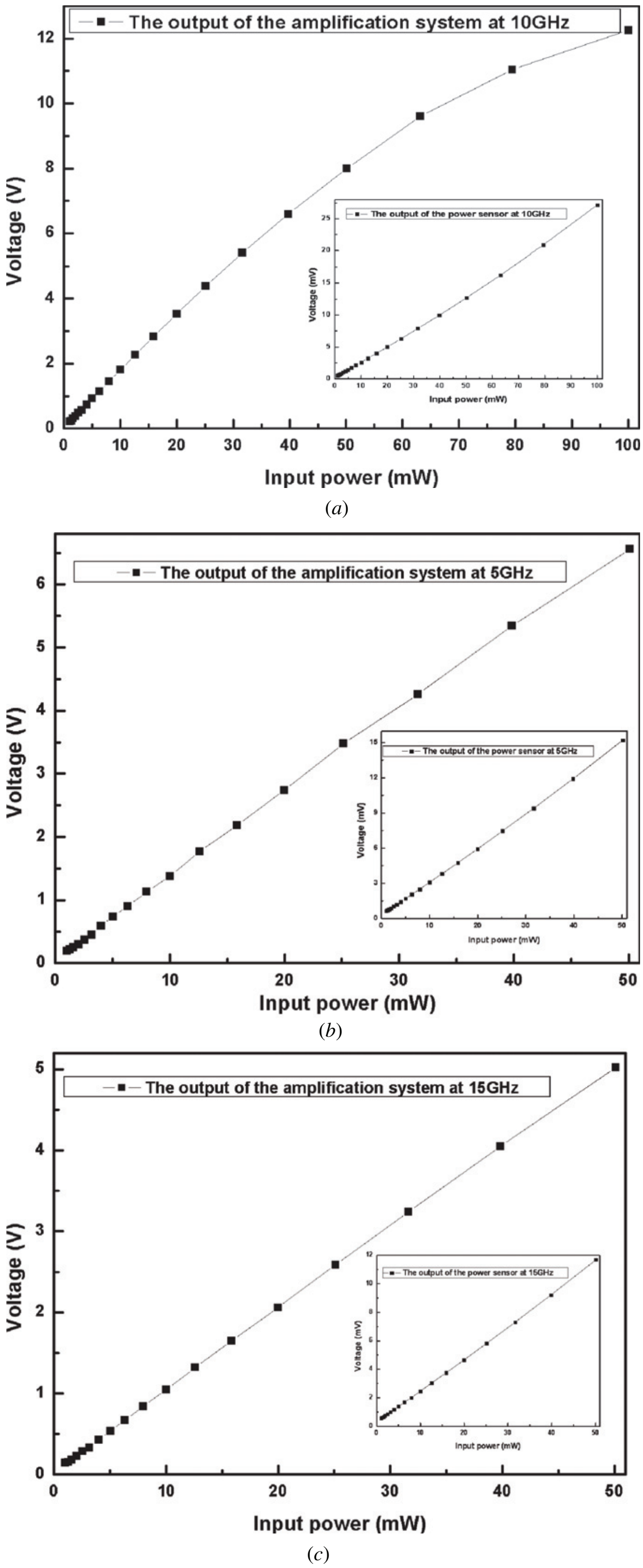

Figure 15. Measured output voltage versus input power characteristics after amplification. (*a*) The measurement result at 10 GHz. (*b*) The measurement result at 5 GHz. (*c*) The measurement result at 15 GHz.

signal of the power sensor well and have good linearity within 50 mW.

5. Conclusion

A terminating-type MEMS microwave power sensor and its amplification system are presented in this paper. The SPICE model is introduced to simulate the temperature distribution of this power sensor. This power sensor is designed and fabricated using MEMS technology and the GaAs MMIC process. The return loss measurement reflects that the power sensor has a good match characteristic. The amplification system consists of an amplifier circuit and a low-pass filter circuit, and the measurement results show that the amplification system can amplify the output weak signal of the power sensor well and have good linearity.

Acknowledgments

This work is supported by the National Natural Science Foundation of China (60976094, 60676043) and the National High Technology Research and Development Program of China (863 Program, 2007AA04Z328).

References

[1] Van Herwaarden A W and Sarro P M 1986 Thermal sensors based on the Seebeck effect *Sensors Actuators* **10** 321–46

[2] Kodato S *et al* 1997 New structure for DC-65 GHz thermal power sensor *Int. Conf. on Solid-State Sensors and Actuators (June 1997)* pp1279–82

[3] Milanovic V *et al* 1997 Thermoelectric power sensor for microwave applications by commercial CMOS fabrication *IEEE Electron Device Lett.* **18** 450–3

[4] Jaeggi D, Baltes H and Moser D 1992 Thermoelectric AC power sensor by CMOS technology *IEEE Electron Device Lett.* **13** 366–8

[5] Dehe A, Krozer V, Chen B and Hartnagel H L 1996 High-sensitivity microwave power sensor for GaAs-MMIC implementation *Electron. Lett.* **32** 2149–50

[6] Lalinsky T *et al* 1999 The improved performance of GaAs micromachined power sensor microsystem *Sensors Actuators* A **76** 241–6

[7] Wang D B and Xiao X P 2009 A novel symmetrical microwave power sensor based on GaAs monolithic microwave integrated circuit technology *J. Micromech. Microeng.* **19** 125012–9 (8pp)

[8] Swart N R and Nathan A 1992 Flow-rate microsensor modeling and optimization using SPICE *Sensors Actuators* A **34** 109–22

[9] Milanovic V *et al* 1999 Optimization of CMOS MEMS microwave power sensors *ISCAS* vol 5 pp 144–7

[10] Kozlov A G 2000 Optimization of thin-film thermoelectric radiation sensor with separate disposition of absorbing layer and comb thermoelectric transducer *Sensors Actuators* A **84** 259–69

[11] Dehe A *et al* 1996 GaAs monolithic integrated microwave power sensor in coplanar waveguide technology *IEEE MTT-S Digest (June 1996)* pp 161–4

[12] Shih K K and Blum J M 1972 Contact resistances of Au-Ge-Ni, Au-Zn and Al to III–V compounds *Solid-State Electron.* **15** 1177–80

[13] George E P *et al* 1999 A measurement-based design equation for the attenuation of MMIC-compatible coplanar waveguides *IEEE Trans. Microw. Theory Tech.* **47** 241–3

[14] Chramiec J, Adamski M E and Kitlihski M 2000 Evaluation of chip resistor CAD models used in microwave circuit design programs *Proc. Int. Conf. on Signals and Electronic Systems ZCSES'2000* pp 369–72